Supplementary Information

for

In-situ Assembly of Wearable Capacitive Sensor with Spine-shaped Dielectric for Shear-Pressure Monitoring

Bing Ji,[a,†] Qian Zhou,[a,†] Ge Chen,[a] Ziyi Dai,[a] Shunbo Li,[b] Yi Xu,[b] Yibo Gao,[c,d] Weijia Wen,[d] and Bingpu Zhou[a,]*

[a]*Joint Key Laboratory of the Ministry of Education, Institute of Applied Physics and Materials Engineering, University of Macau, Avenida da Universidade, Taipa, Macau 999078, China*

[b]*Key Laboratory of Optoelectronic Technology and Systems, Ministry of Education & Key Disciplines Laboratory of Novel Micro-Nano Devices and System Technology, College of Optoelectronics Engineering, Chongqing University, Chongqing 400044, China*

[c]*Shenzhen Shineway Hi-Tech Corporation, Shenzhen 518112, China*

[d]*Department of Physics, The Hong Kong University of Science and Technology, Clear Water Bay, Kowloon, Hong Kong 999077*

[†]*Bing Ji and Qian Zhou contributed equally to this work.*

Keywords: Electronic skin, pressure sensor, shear force, spine dielectric.

Corresponding Author

Bingpu Zhou, Email: bpzhou@um.edu.mo. Fax: +853-88222426. Tel: +853-88224196.

Supplementary figures.

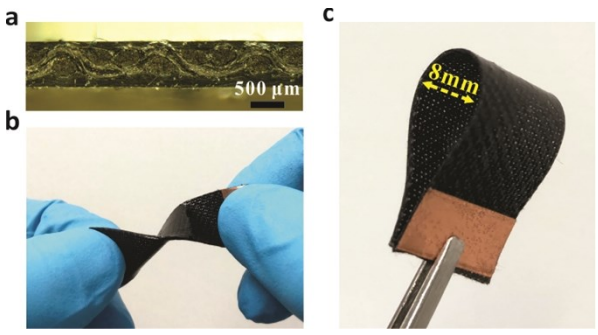

SFigure 1. a) Cross-sectional optical image of the carbon fabric electrode with PDMS encapsulation. b) and c) The flexibility of the PDMS encapsulated carbon fabric electrode.

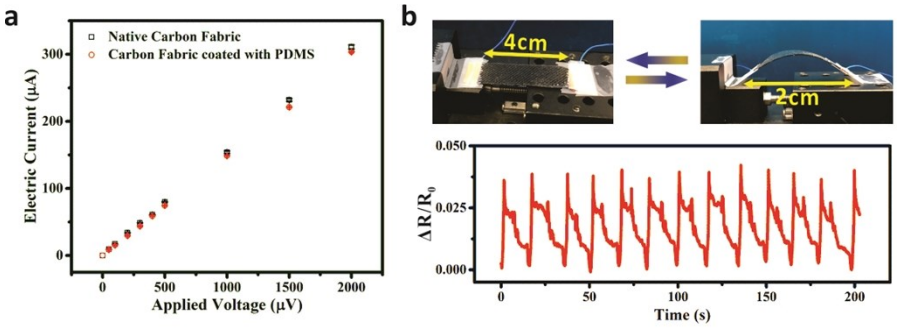

SFigure 2. a) Comparison of the current as a function of the applied voltage for the carbon fabric with and without the PDMS encapsulation. The length and width of the electrode for test are 4 cm and 1 cm, respectively. b) Measurement of the electric resistance stability of the carbon fabric electrode via periodical bending and release.

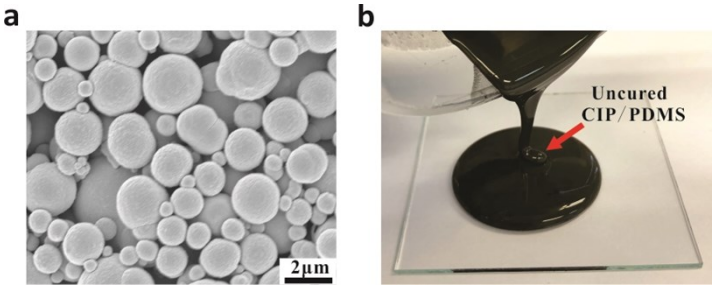

SFigure 3. a) SEM image of the carbonyl iron particles. b) Photograph of the uncured mixed gel of CIP and PDMS.

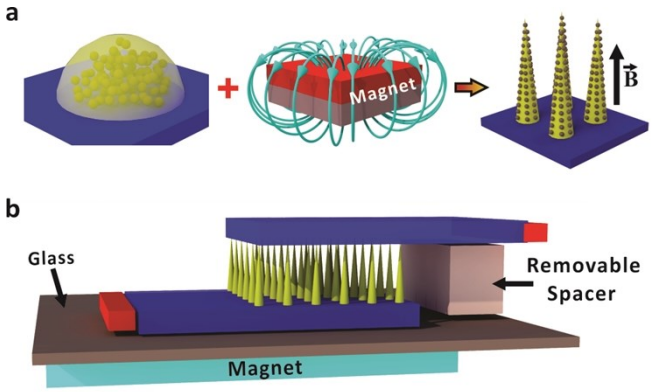

SFigure 4. a) Mechanism of the spine formation when the magnetic CIP/PDMS gel was applied with the external magnetic field. b) Schematic of the experimental setup for in-situ assembly of the dual-mode flexible sensor.

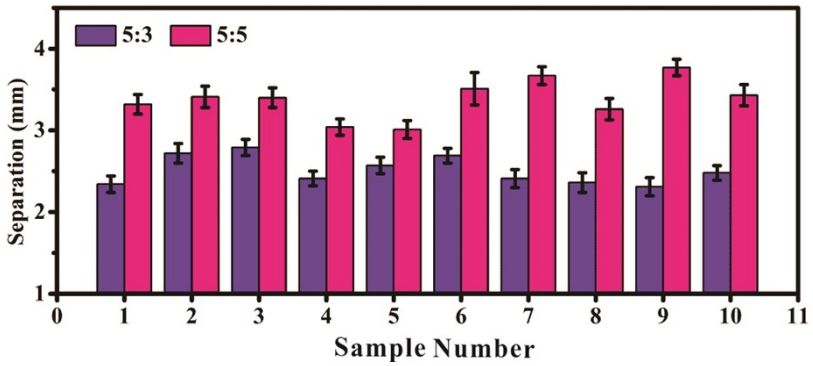

SFigure 5. Comparison of electrode separation of the assembled sensors prepared by dielectric of 5:3 and 5:5 from ten different samples, respectively.

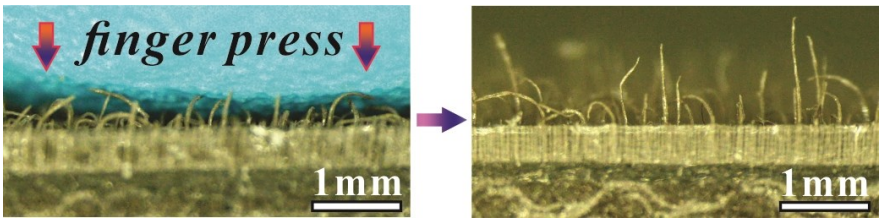

SFigure 6. The optical images of the spine shapes prepared from mass ratio of 5:1 and the related mechanical behavior after finger pressing (right panel).

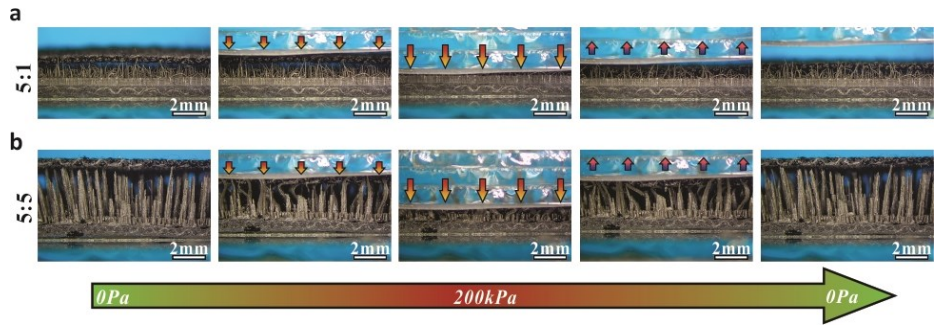

SFigure 7. Cross-sectional optical images of the dielectric deformation prepared by mass ratio of a) 5:1 and b) 5:5 under varying pressure from 0 Pa to 200 kPa, and finally returned to 0 Pa.

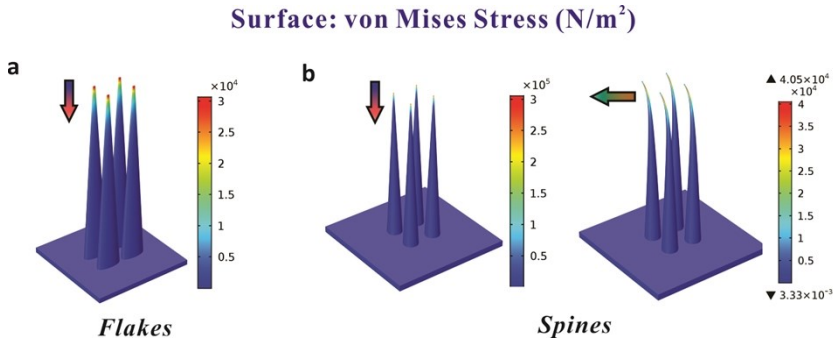

SFigure 8. Simulation results showing the surface stress from a) flakes with force in downward direction, and b) spines with force in the downward and horizontal directions.

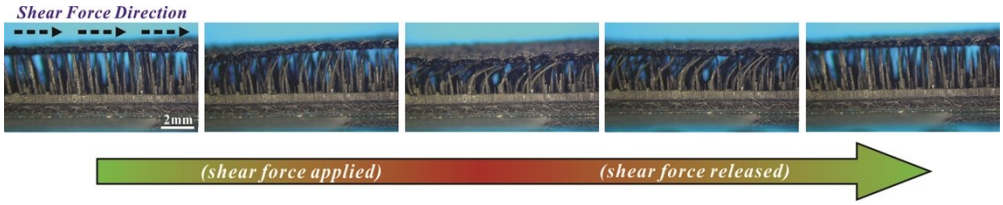

SFigure 9. The cyclic structural deformation of the spine-shaped dielectric with applied shear force towards to the right.

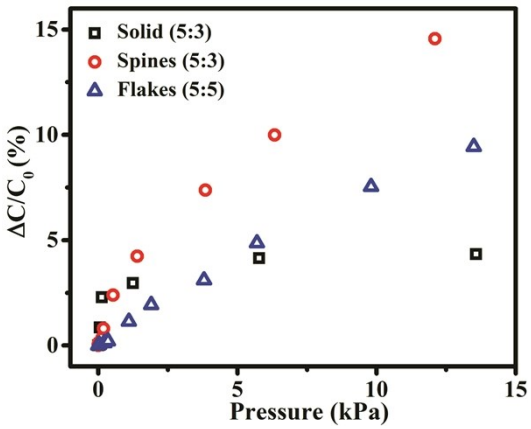

SFigure 10. Close-up capacitance variation as a function of the applied pressure from different sensors within pressure range of 0 - 15 kPa.

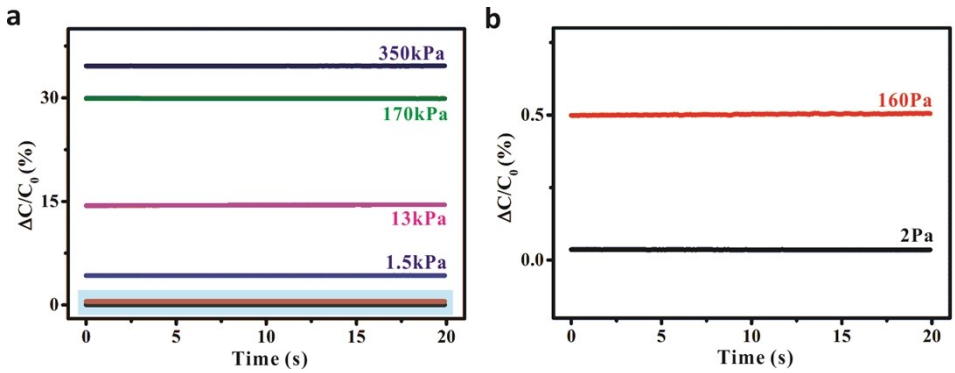

SFigure 11. a) Monitoring of the relative capacitance change under different applied pressures of 2 Pa, 160 Pa, 1.5 kPa, 13 kPa, 170 kPa, and 350 kPa, for duration of 20 s. A close-up image of the curves in light blue region for pressure of 2 Pa and 160 Pa is shown in (b).

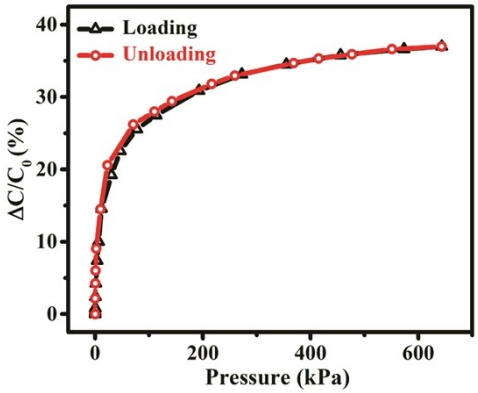

SFigure 12. The capacitance response of the pressure sensor in a loading (black curve) and unloading (red curve) cycle.

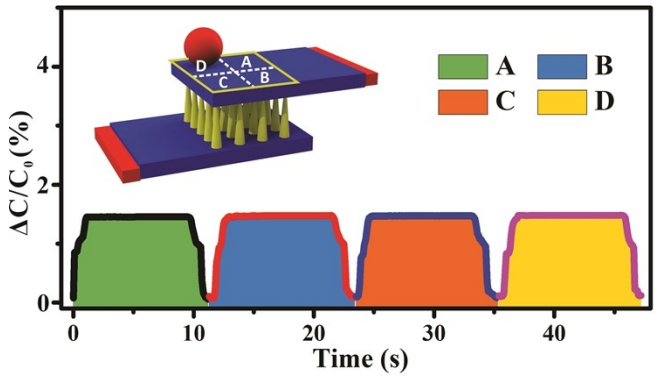

SFigure 13. Uniformity test via placing a steel ball (mass of 0.5 g) onto four identical regions of the assembled sensor. The total sensing window (1 cm ⊘ 1 cm) of the device was divided into four regions, A, B, C, and D, with the same area (0.5 cm ⊘ 0.5 cm) for uniformity measurement.

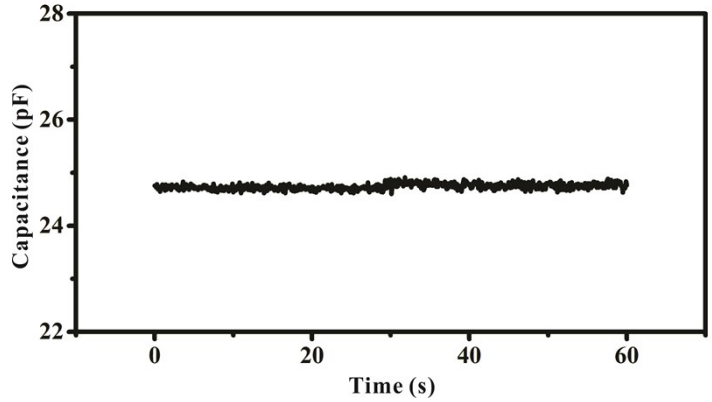

SFigure 14. The base capacitance record for one minute from a typical flexible pressure sensor with the spine dielectric prepared from mass ratio of 5:3.

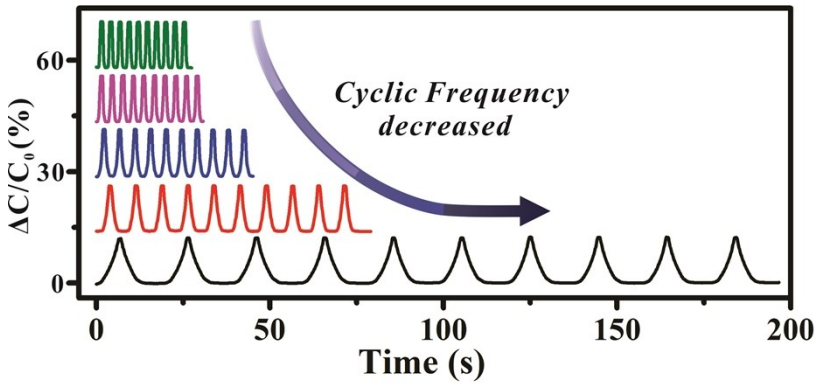

SFigure 15. Capacitance variation under different cyclic frequencies with pressure loading and release. The maximum pressure applied for the measurement is 12 kPa.

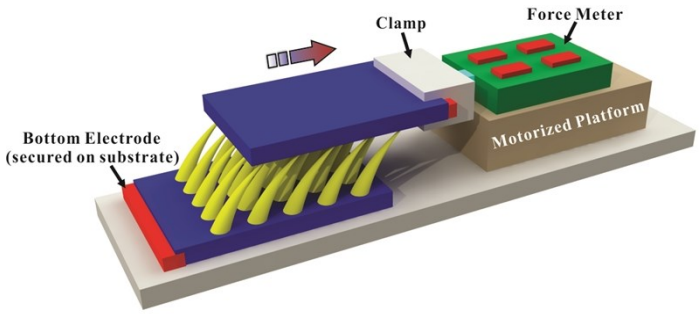

SFigure 16. Schematic illustration of the experimental setup for shear force test. A force meter was fixed with the top electrode via a clamp, along with the motorized platform to induce shear force onto the assembled sensor.

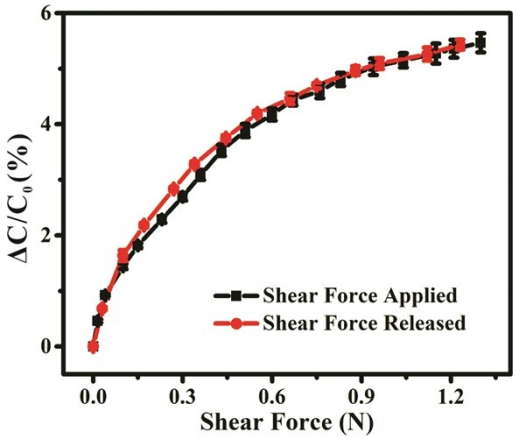

SFigure 17. The capacitance response of the sensor for shear force detection in an applying (black curve) and releasing (red curve) cycle.

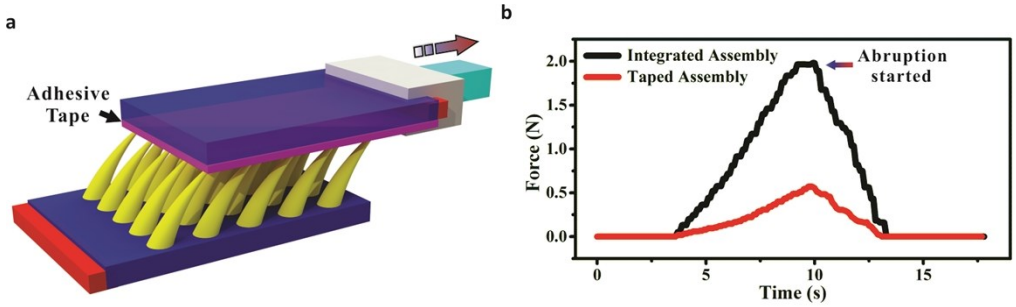

SFigure 18. a) Schematic of the sensor assembled with assistance of the adhesive tape that is inserted between the apex of the spines and the top electrode. b) The pulling force to induce shear deformation and abruption of the assembled sensor as a function of the time.

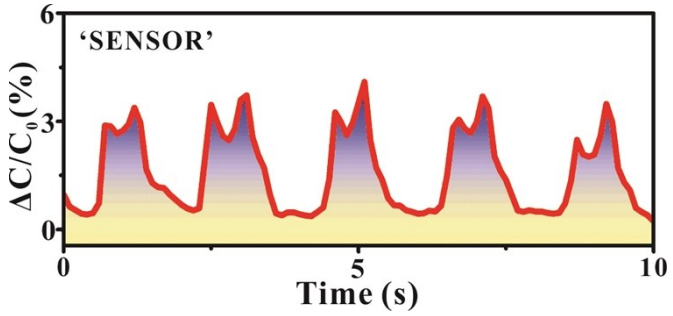

SFigure 19. Real-time monitoring of the voice vibrations during the pronunciations of the word 'sensor'.

Section S1: Establishment of COMSOL model.

The model was established in a three-dimensional structure using COMSOL Multiphysics software. The 4 × 4 cone array and elliptical cone array with similar size as the experiments were employed to simulate the spine and flake structures, respectively. The cone was defined with the bottom diameter of 250 μm, top diameter of 10 μm, height of 2500 μm and center distance of 425 μm for the cone array. The bottom size of the elliptical cone was set with the major-axis diameter of 500 μm and minor-axis diameter of 200 μm. The apex size of the elliptical cone was set as 0.1 times of the bottom size. The center distance of 550 μm (major-axis direction) and 400 μm (minor-axis direction) was employed for the elliptical cone array. PDMS with the default parameter (density of 970 kg/m^3, Young's modulus of 750 kPa and Poisson's ratio of 0.49) was employed as the elastic materials in the model.

The Solid Mechanics module was selected to trace the stress distribution and displacement, with the governing equation $\nabla \cdot S + Fv = 0$. In the equation, Fv is the volume force vector and $S = C : \varepsilon$, where $C = C\ (E,v)$ is a parameter of materials related to the Yong's modulus E and the Poisson's ratio v, and $\varepsilon = \frac{1}{2}[(\nabla u)^T + \nabla u]$ is the strain related to the displacement vector $\boldsymbol{u}$. The model was mainly established to clarify the deformation capability of spine and flake structures. The large deformation issue was not involved in this model and thus the static mesh was selected. By applying vertical (1×10^{-4} N) and horizontal forces (1×10^{-6} N), the stress and displacement of both the spine array and flake array were analyzed and compared. The localized stress and more obvious displacement of spine structure reflect the better deformation capability, which promises

the high sensitivity of sensor based on the spine-shaped dielectric as exhibited from the experimental results.

Section S2: Derivation and comparison of the pressure sensitivity.

The sensitivity of the pressure sensor as a function of the applied pressure can be defined by

$$S = \frac{\partial(\Delta C / C_0)}{\partial P}$$

where $\Delta C / C_0$ is the relative capacitance variation and ***P*** the applied normal pressure. The relative capacitance variation can be expressed as

$$\frac{\Delta C}{C_0} = \frac{C - C_0}{C_0} = \frac{C}{C_0} - 1$$

where C_0 is the initial capacitance without pressure and C the resultant capacitance when external pressure was applied. The capacitance of parallel plate capacitor is normally defined by

$$C = \frac{\varepsilon A}{d}$$

where ε is the dielectric constant, d the distance between the facing electrodes and A the overlapping area of the electrodes. For two-phased composite materials, the overall dielectric constant can be simply expressed as[1-2]

$$\varepsilon = \varepsilon_a f_a + \varepsilon_b f_b$$

where ε_a and ε_b are the intrinsic dielectric constant of the individual material, and f_a and f_b are the corresponding volume fraction (herein, the subscript a represents air and b represents the CIP/PDMS component). The initial and resultant dielectric constant can be expressed as

$$\varepsilon_0 = \varepsilon_a f_a + \varepsilon_b f_b = \varepsilon_a(1 - f_b) + \varepsilon_b f_b = \varepsilon_a + f_{b0}(\varepsilon_b - \varepsilon_a)$$

$$\varepsilon = \varepsilon_a f_a + \varepsilon_b f_b = \varepsilon_a(1 - f_b) + \varepsilon_b f_b = \varepsilon_a + f_b(\varepsilon_b - \varepsilon_a)$$

We then can compare the sensitivity under the same applied pressure as of

$$\frac{\Delta C}{C_0} = \frac{C}{C_0} - 1 = \frac{\varepsilon A / d}{\varepsilon_0 A / d_0} - 1 = \frac{\varepsilon_a + f_b(\varepsilon_b - \varepsilon_a)}{\varepsilon_a + f_{b0}(\varepsilon_b - \varepsilon_a)} \cdot \frac{d_0}{d} - 1$$

Under the relatively lower pressure range, it is reasonable to consider that the volume fraction of the CIP/PDMS remains almost unchanged. We then have

$$f_b \approx f_{b0}$$

Also,

$$\frac{d_0}{d} = \frac{d_0}{d_0 - \Delta d} = \frac{1}{1 - \Delta d/d_0}$$

where ***Δd*** is the compressed distance during the application of the pressure. As shown in **Figure 2a**, the value of d_0 from 5:5 is larger than that from 5:3. Also, the value of ***Δd*** from 5:5 is smaller than that from 5:3 as presented in **Figure 2f** and **Figure 2h**. Consequently, the value of $\frac{d_0}{d}$ is relatively smaller from 5:5 when compared with that from 5:3. The results herein confirm that the sensitivity under lower pressure range is higher for the sensor with dielectric prepared from mass ratio of 5:3 as shown in **Figure 3b**.

Reference:

1. S. R. A. Ruth, L. Beker, H. Tran, V. R. Feig, N. Matsuhisa and Z. Bao, *Adv. Funct. Mater.,* 2019, 1903011.

2. Y. Wan, Z. Qiu, J. Huang, J. Yang, Q. Wang, P. Lu, J. Yang, J. Zhang, S. Huang, Z. Wu and C. F. Guo, *Small,* 2018, **14**, e1801657.